A Self-Consistent Solution of the Poisson, Schrödinger and Boltzmann Equations for GaAs Devices by a Deterministic Solver

Zeinab Kargar*, Dino Ruić and Christoph Jungemann
Chair of Electromagnetic Theory
RWTH Aachen University
52056 Aachen, Germany
*Email: zk@ithe.rwth-aachen.de

***Abstract*—A deterministic solver based on the Fourier harmonics expansion of the Boltzmann equation is applied to the case of GaAs devices including polar optical phonon scattering and the Pauli principle. The system of the Poisson, Schrödinger and Boltzmann equations is solved self-consistently. Results are presented for a double-gate nMOSFET which shows a velocity overshoot in the channel region and electrons lose their energy by an optical phonon cascade.**

I. Introduction

As semiconductor device sizes shrink below $100nm$, velocity overshoot starts to dominate the device behavior. This effect can not be predicted by the conventional drift-diffusion model and subsequently the drain current is underestimated in transistors [1]. The Boltzmann equation describes the carrier transport in phase space and gives more accurate information about the device operation than the drift-diffusion model or any extensions thereof which are derived as moments of the Boltzmann equation [2]. In recent years, new methods have been developed to solve the Boltzmann equation deterministically without the stochastic errors and the transiency associated with Monte Carlo simulations [3], [4]. A deterministic solver for silicon devices based on a self-consistent solution of the Poisson equation (PE), Schrödinger equation (SE) and Boltzmann equation (BE) with a Fourier harmonics expansion of the $\boldsymbol{k}$-space for electrons has been successfully developed in Ref. [5]. In GaAs devices, electrons interact with the lattice predominantly by polar optical phonon scattering due to the polar nature of the bonding between Ga and As atoms. Its Fourier harmonics expansion is much more complicated than that of the non-polar phonon scattering mechanisms in silicon.

In this work, we present a deterministic solver based on the Fourier harmonics expansion for a double-gate nMOSFET with a GaAs channel which includes the Pauli principle and polar optical phonon scattering.

II. Approach

The scattering term $S^\nu\{f\}$ of the BE is given by the single particle scattering integral including the Pauli principle:

$$\hat{S}^\nu\{f\} = \frac{1}{(2\pi)^2}\sum_{\nu',\eta,\sigma}\int\Big\{(1-f^\nu(y,\boldsymbol{k}))S^{\nu,\nu'}_{\eta,\sigma}(y,\boldsymbol{k},\boldsymbol{k}')f^{\nu'}(y,\boldsymbol{k}') - (1-f^{\nu'}(y,\boldsymbol{k}'))S^{\nu',\nu}_{\eta,-\sigma}(y,\boldsymbol{k}',\boldsymbol{k})f^{\nu}(y,\boldsymbol{k})\Big\}\,\mathrm{d}^2k', \quad (1)$$

where the transition rate $S^{\nu,\nu'}_{\eta,\sigma}$ is given by:

$$S^{\nu,\nu'}_{\eta,\sigma}(y,\boldsymbol{k},\boldsymbol{k}') = c^{\nu,\nu'}_{\eta,\sigma}(y,\boldsymbol{k},\boldsymbol{k}')\delta(\varepsilon^\nu(\boldsymbol{k}) - \varepsilon^{\nu'}(\boldsymbol{k}') - \sigma), \quad (2)$$

where η runs over all scattering mechanisms, c is the transition coefficient from the initial state with the wave vector $\boldsymbol{k}'$ in the subband ν' to the final state with the wave vector $\boldsymbol{k}$ in the subband ν with a constant energy transfer $\sigma = \pm\hbar\omega_\eta$. The projection of the scattering term onto Fourier harmonics and additionally onto an equi-energy surface is expressed as [6]

$$\hat{S}^\nu\{f\} \to \hat{S}^\nu_m(y,\tilde{\varepsilon}) = \frac{1}{(2\pi)^2}\int\hat{S}^\nu\{f\}\delta(\tilde{\varepsilon}-\tilde{\varepsilon}^\nu(y,\boldsymbol{k}))Y_m(\phi)\mathrm{d}^2k. \quad (3)$$

Afterwards, the kinetic energies are transformed into total energies H by the H-transformation [4]. The scattering term is split into in- and out-scattering. Projection of the in-scattering term yields:

$$\hat{S}^{\nu,in}_m(y,H) = \sum_{\nu',\eta,\sigma}\sum_{m',m''=-\infty}^{\infty} c^{\nu,\nu'}_{m',\eta,\sigma}(y,H)a_{m,m',m''} \times\Big(Z^\nu_0(y,H)\delta_{0,m''} - Y_0 Z^\nu_0(y,H)\; f^\nu_{m''}(y,H)\Big) \times\; Y_0\; Z^{\nu'}_0(y,\bar{H}_\sigma(H))f^{\nu'}_{m'}(y,\bar{H}_\sigma(H)), \quad (4)$$

and projection of the out-scattering yields:

$$\hat{S}^{\nu,out}_m(y,H) = \sum_{\nu',\eta,\sigma}\sum_{m',m''=-\infty}^{\infty} c^{\nu',\nu}_{m'',\eta,\sigma}(y,\bar{H}_{-\sigma}(H))a_{m,m',m''} \times\Big(Z^{\nu'}_0(y,\bar{H}_{-\sigma}(H))\delta_{0,m''} - Y_0\; Z^{\nu'}_0(y,\bar{H}_{-\sigma}(H))f^{\nu'}_{m''}(y,\bar{H}_{-\sigma}(H))\Big) \times Y_0\; Z^\nu_0(y,H)f^\nu_{m'}(H)), \quad (5)$$

where $\bar{H}_\sigma = H + \sigma$. We approximate the band structure for GaAs to be isotropic, therefore the density of states is independent of the angle and all expansion coefficients vanish except for the zeroth order, $Z^\nu_0(y,H)$. The integral of products of Fourier harmonics $a_{m,m',m''}$ is:

$$a_{m,m',m''} = \int_0^{2\pi} Y_m(\phi)Y_{m'}(\phi)Y_{m''}(\phi)\;\mathrm{d}\phi.$$

When the transition rate depends on the angle between the initial and final wave vectors, like polar optical phonon scattering, higher order expansions of the transition rate must be considered. The non-polar phonon scatterings, like acoustic

978-1-4673-7860-4/15/$31.00 ©2015 IEEE

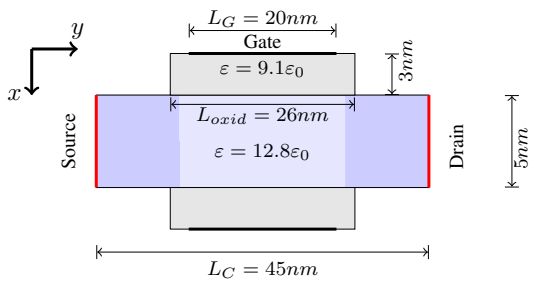

Fig. 1. Double-gate nMOSFET with a GaAs channel.

and inter-valley phonon scattering [7], can be treated as velocity randomizing hence only the zeroth harmonic, c_0 in Eqs. (4) and (5) contributes.

The scattering coefficient of the polar optical phonon scattering can be expressed as $c_m = \gamma_0(\bar{c}_m + \bar{c}_{-m} - \delta_{0,m}\bar{c}_m)$. The constant part of this coefficient is given by [7]

$$\gamma_0 = \frac{\pi\,\omega_{ph}e^2}{2}\,(\frac{1}{\epsilon_\infty} - \frac{1}{\epsilon_s})(n_{ph} + \frac{1}{2} \pm \frac{1}{2}),$$

where ω_{ph} is the angular frequency of the polar optical phonon, the phonon number n_{ph} is given by the Bose-Einstein distribution, and ϵ_∞ and ϵ_s are the high frequency and static dielectric constant, respectively. The second part of the scattering coefficient c_m depends on the harmonics and energies.

$$\bar{c}_m(k,k') = \int_0^{2\pi} \frac{F_{\nu,\nu'}(q)}{q} Y_m(\phi_{k,k'})\; d(\phi_{k,k'}), \qquad (6)$$

where

$$q^2 = k^2 + k'^2 - 2kk'\cos(\phi_{k,k'}),$$
$$F_{\nu,\nu'}(q) = \int_x \int_{x'} \xi^\dagger_\nu(x)\xi_{\nu'}(x)\xi^\dagger_\nu(x')\xi_{\nu'}(x')e^{-q|x-x'|}dx'dx, \qquad (7)$$

with the normalized wave function $\xi(x)$. Thus, the polar optical phonon interaction is an intra-valley, inelastic and anisotropic interaction.

The boundary condition for source and drain contacts in the BE is of the Neumann-type together with a surface generation rate. After an expansion onto Fourier harmonics it reads [8]:

$$\Gamma^\nu_m(\mathrm{y},H) = \; Z^\nu_0 f^{eq}_0(y,H) \int_0^{2\pi} \Theta(\mathbf{v}\cdot\mathbf{n})\mathbf{v}\cdot\mathbf{n}\, Y_0(\phi)Y_m(\phi)\mathrm{d}\phi$$
$$+Z^\nu_0 \sum_{m'=-\infty}^{\infty} f^\nu_{m'}(y,H) \int_0^{2\pi} \Theta(-\mathbf{v}\cdot\mathbf{n})\mathbf{v}\cdot\mathbf{n}\, Y_{m'}(\phi)\; Y_m(\phi)\mathrm{d}\phi, \qquad (8)$$

where $\mathbf{n}$ is a surface vector pointing into the device, $\mathbf{v}$ the group velocity and $\Theta(x)$ the Heaviside function.

III. Results

Results are presented for a 2D double-gate nMOSFET with a GaAs channel, as shown in Fig. 1. The device is homogeneous in z-direction. The grid is equidistant with a grid spacing of $0.2nm$ in x-direction, and $0.6nm$ in y-direction. The nonparabolic conduction band of GaAs comprises the Γ-valley in the center of the first Brillouin zone, four equivalent

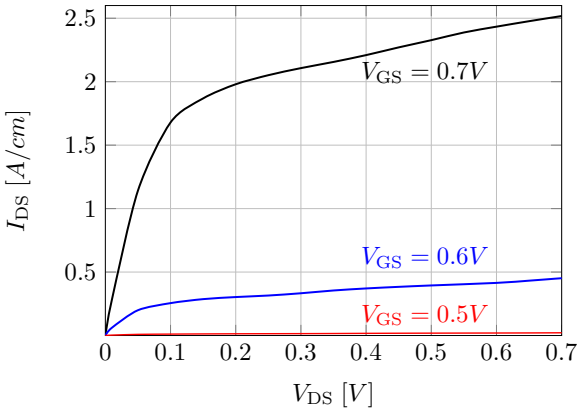

Fig. 2. Stationary drain current I_{DS} vs. drain bias V_{DS} at $V_{GS} = 0.7V,\ 0.6V,\ 0.5V$.

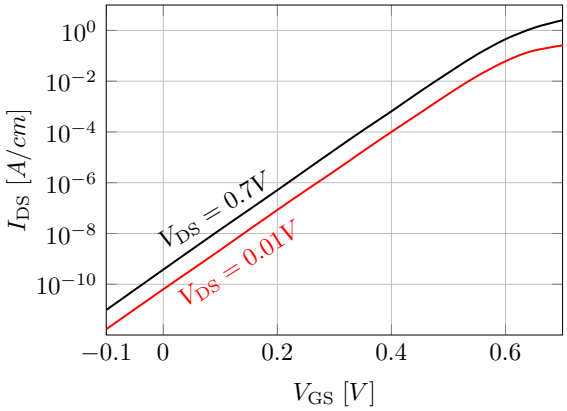

Fig. 3. Stationary drain current I_{DS} vs. gate bias V_{GS}, at $V_{DS} = 0.7V$ and $V_{DS} = 0.01V$

L-valleys, and three equivalent X-valleys. The doping profile of the device including a gate underlap of $1nm$, a slope of $1\frac{nm}{dec}$, and a maximum value of $5 \cdot 10^{19}cm^{-3}$ is shown in Fig. 4. We use the material parameters reported in [9] for GaAs.

The SE is solved in the GaAs channel in x-direction (confinement direction), while the BE is set up in y-direction (transport direction) in the real space and 2D $\boldsymbol{k}$-space, with an energy grid spacing of $6meV$ and the five lowest subbands are included. The scattering term consists of intra-valley elastic acoustic phonon and inter-valley phonon scattering, both of which are approximated as velocity randomizing, and intra-valley polar optical phonon scattering.

To compute the potential, subband energies, and wave functions, the PE and SE are solved until self-consistency is reached. Thereafter the PE, SE, and BE are solved self-consistently by the Gummel iteration method [10].

The drain current versus drain bias at a gate bias of $V_{GS} = 0.5V$, $0.6V$, and $0.7V$ is plotted in Fig. 2 while the resulting drain current versus gate bias at a drain bias of $V_{DS} = 0.01V$ and $0.7V$ is depicted in Fig. 3. The electron density integrated in the confinement direction is plotted in Fig. 4 at a drain bias of $V_{DS} = 0.7V$ for various gate biases. The fraction of electrons in the lowest subband of the Γ-, L-, and X-valleys is shown in Fig. 5. These three subbands contain

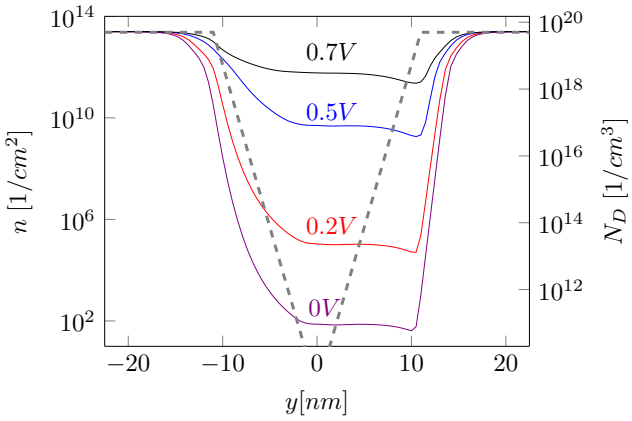

Fig. 4. Electron densities integrated in the confinement direction (solid lines; left axis) for $V_{\mathrm{DS}} = 0.7V$ and $V_{\mathrm{GS}} = 0V,\ 0.2V,\ 0.5V,\ 0.7V$ together with the doping density N_{D} (dashed line; right axis).

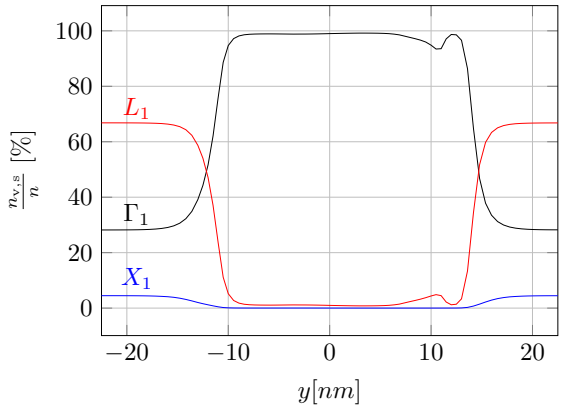

Fig. 5. Fraction of electrons in the minimum subband of the Γ-, L-, and X-valleys for $V_{\mathrm{DS}} = 0.7V$ and $V_{\mathrm{GS}} = 0.5V$.

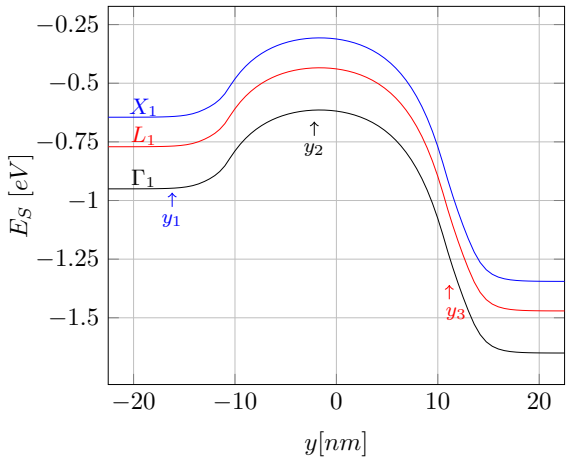

Fig. 6. Minimum subband energy of the Γ-, L-, and X- valleys vs position for $V_{\mathrm{DS}} = 0.7V$ and $V_{\mathrm{GS}} = 0.5V$.

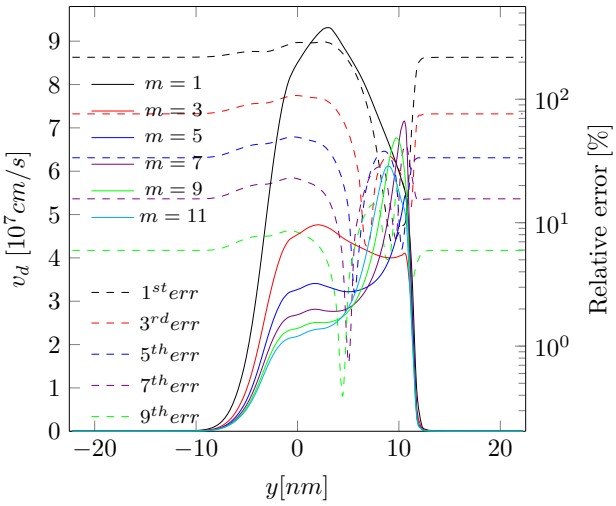

Fig. 7. Drift velocity and its relative error at $V_{\mathrm{DS}} = 0.7V$ and $V_{\mathrm{GS}} = 0.5V$ for different maximum expansion orders.

more than 99% of all electrons. In the source and drain most electrons are in the four L-valleys because the Pauli principle pushes the particles to higher energies and the four L-valleys have a higher mass than the single Γ-valley and therefore a much higher density of states. Under the gate the electron density is much smaller and due to the lower energy of the lowest subband in the Γ-valley almost all electrons reside in the Γ-valley. Only at the end of the channel some electrons are scattered into the L-valleys leading to a small dip in the electron density in the Γ-valley at about $y = 10nm$. Thus, the electron transport happens mostly in the lowest subband of the Γ-valley, because this subband has the lowest barrier with respect to total energy in the channel. The band edge of the lowest subband of the Γ-, L-, and X-valleys is depicted in Fig. 6

In Fig. 7 the drift velocity and its relative error are depicted for different maximum expansion orders of the Fourier harmonics relative to a eleventh order expansion. The lowest expansion order overestimates the velocity very much and a rather high order is required to capture all aspects of the quasi-ballistic transport. In Fig. 8 the drift velocity in the channel region in transport direction is plotted for different gate biases. In such a small device the length of the gate is comparable to or smaller than the mean free path. For this reason carriers move quasi-ballistically and a velocity overshoot occurs under the gate [11]. This velocity overshoot is related to the quasi-ballistic transport and not to the transfer of electrons from the Γ-valley to the L-valleys (cf. Fig. 5).

Fig. 9 shows the electron energy distribution function for different positions in the transport direction which are marked in Fig. 6. The distribution function for position y_1 is close to the Fermi-Dirac distribution function because of the inclusion of the Pauli principle. In Fig. 9 the zigzag behavior in the distribution function is due to scattering by optical phonons and the energy difference between adjacent maxima is equal to the energy of the optical phonons. This is known as the phonon cascade [12].

IV. Conclusion

We have developed the first deterministic Boltzmann-Schrödinger-Poisson solver for III-V materials which includes the Pauli principle and polar optical phonon scattering. The results show a velocity overshoot in the device and the transport

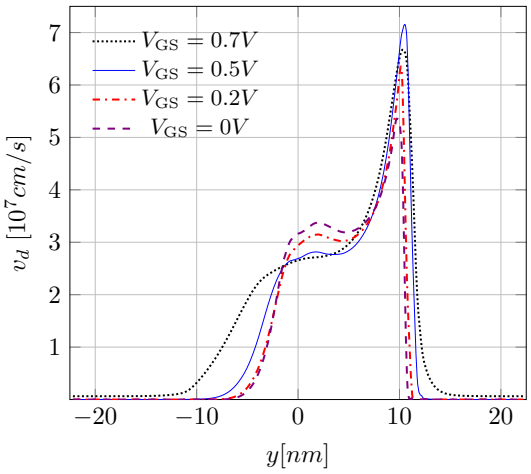

Fig. 8. Drift velocity for $V_{\mathrm{DS}} = 0.7V$ and $V_{\mathrm{GS}} = 0V,\ 0.2V,\ 0.5V,\ 0.7V$.

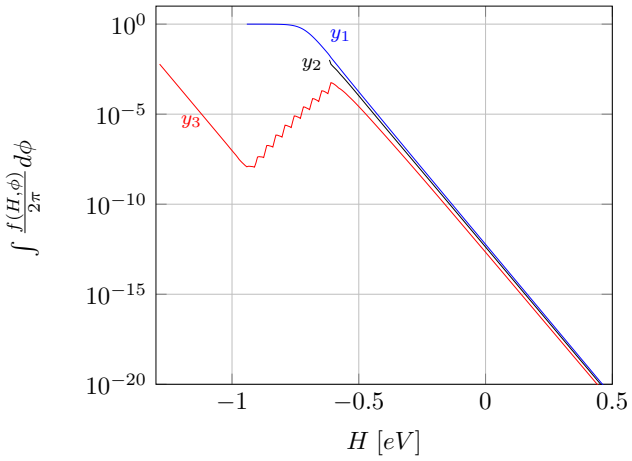

Fig. 9. Energy distribution function of the lowest subband of the Γ valley vs total energy at different positions which are marked in Fig. 6 for $V_{\mathrm{DS}} = 0.7V$ and $V_{\mathrm{GS}} = 0.5V$

in this small device is predominantly quasi-ballistic.

ACKNOWLEDGMENT

Funding by the Deutsche Forschungsgemeinschaft (Ref. No.: JU406/9-1, ME1590/7-1) is gratefully acknowledged.

REFERENCES

[1] W.-S. Choi, F. Assaderaghi, Y.-J. Park, H.-S. Min, C. Hu, and R. W. Dutton, "Simulation of deep submicron SOI N-MOSFET considering the velocity overshoot effect," *Electron Device Letters, IEEE*, vol. 16, no. 7, pp. 333–335, 1995.

[2] T. Grasser, T.-W. Tang, H. Kosina, and S. Selberherr, "A review of hydrodynamic and energy-transport models for semiconductor device simulation," *Proc. IEEE*, vol. 91, no. 2, pp. 251–274, 2003.

[3] M. Galler and F. Schürrer, "A direct multigroup-WENO solver for the 2D non-stationary Boltzmann-Poisson system for GaAs devices: GaAs-MESFET," *Journal of Computational Physics*, vol. 212, pp. 778–797, 2006.

[4] A. Gnudi, D. Ventura, G. Baccarani, and F. Odeh, "Two-dimensional MOSFET simulation by means of a multidimensional spherical harmonics expansion of the Boltzmann transport equation," *Solid–State Electron.*, vol. 36, no. 4, pp. 575 – 581, 1993.

[5] D. Ruić and C. Jungemann, "Numerical aspects of noise simulation in MOSFETs by a Langevin-Boltzmann solver," *Journal of Computational Electronics*, vol. 14, no. 1, pp. 21–36, 2015.

[6] S.-M. Hong, A. T. Pham, and C. Jungemann, *Deterministic solvers for the Boltzmann transport equation*. Computational Microelectronics, Wien, New York: Springer, 2011.

[7] D. Esseni, P. Palestri, and L. Selmi, *Nanoscale MOS Transistors. Semi-Classical Transport and Applications*. Cambridge University Press, 2011.

[8] S.-M. Hong and C. Jungemann, "A fully coupled scheme for a Boltzmann-Poisson equation solver based on a spherical harmonics expansion," *J. Computational Electronics*, vol. 8, no. 3, pp. 225–241, 2009.

[9] J. Požela and A. Reklaitis, "Electron transport properties in GaAs at high electric fields," *Solid-State Electronics*, vol. 23, no. 9, pp. 927–933, 1980.

[10] L. Lucci, P. Palestri, D. Esseni, L. Bergagnini, and L. Selmi, "Multi-subband Monte Carlo study of transport, quantization, and electron-gas degeneration in ultrathin SOI n-MOSFETs," *Electron Devices, IEEE Transactions on*, vol. 54, pp. 1156–1164, 2007.

[11] M. Lundstrom and Z. Ren, "Essential physics of carrier transport in nanoscale MOSFETs," *Electron Devices, IEEE Transactions on*, vol. 49, no. 1, pp. 133–141, 2002.

[12] J. Shah, B. Deveaud, T. Damen, W. Tsang, A. Gossard, and P. Lugli, "Determination of intervalley scattering rates in GaAs by subpicosecond luminescence spectroscopy," *Physical review letters*, vol. 59, no. 19, p. 2222, 1987.